

FIG. 1

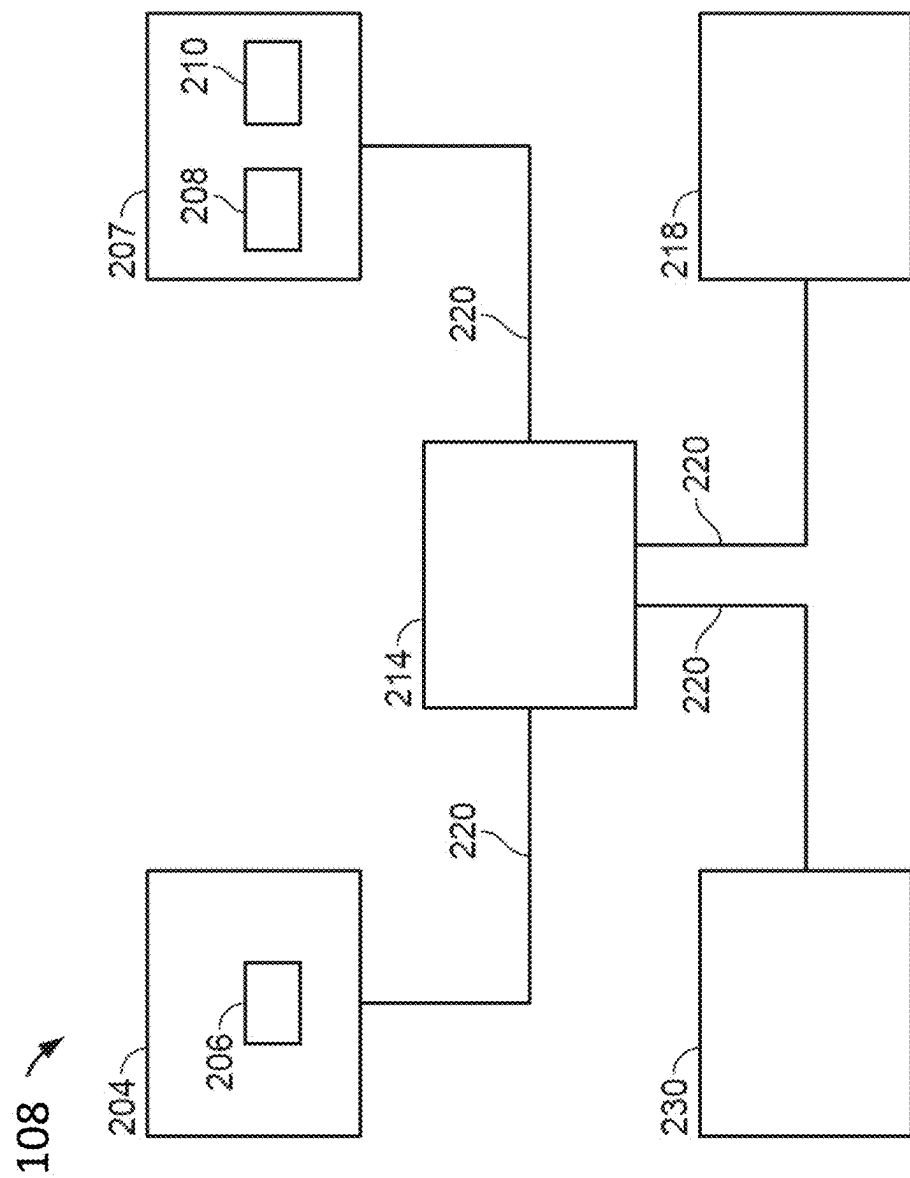


FIG. 2

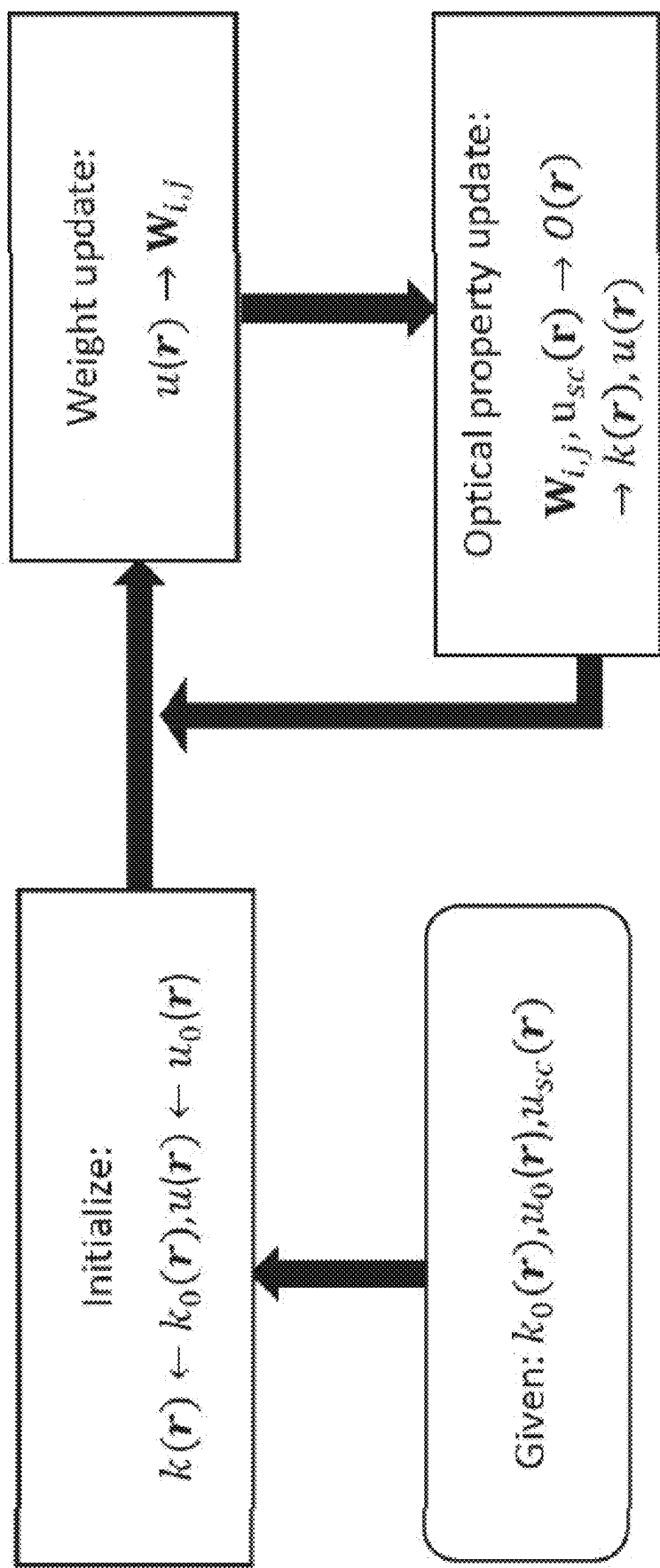


FIG. 3A

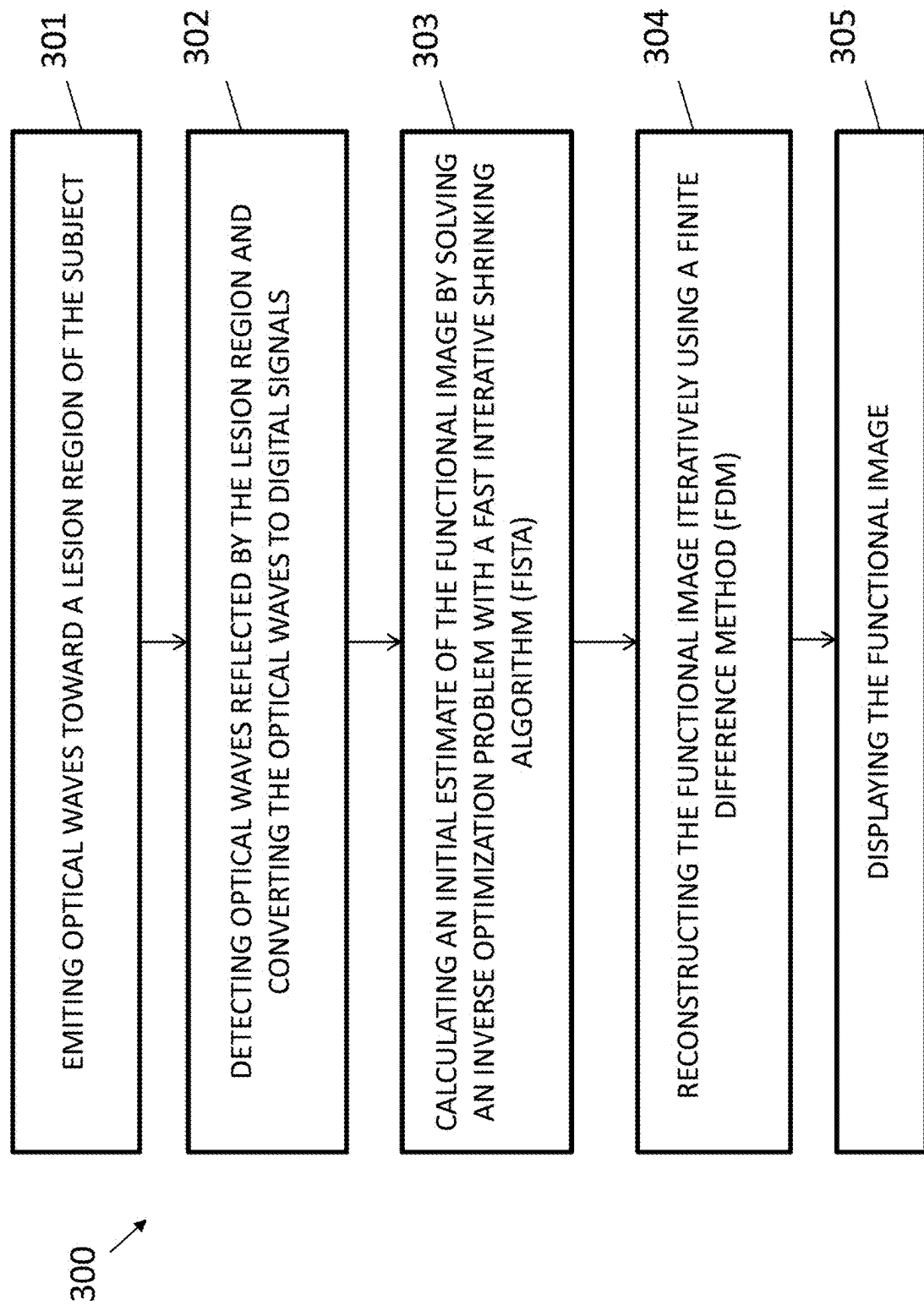


FIG. 3B

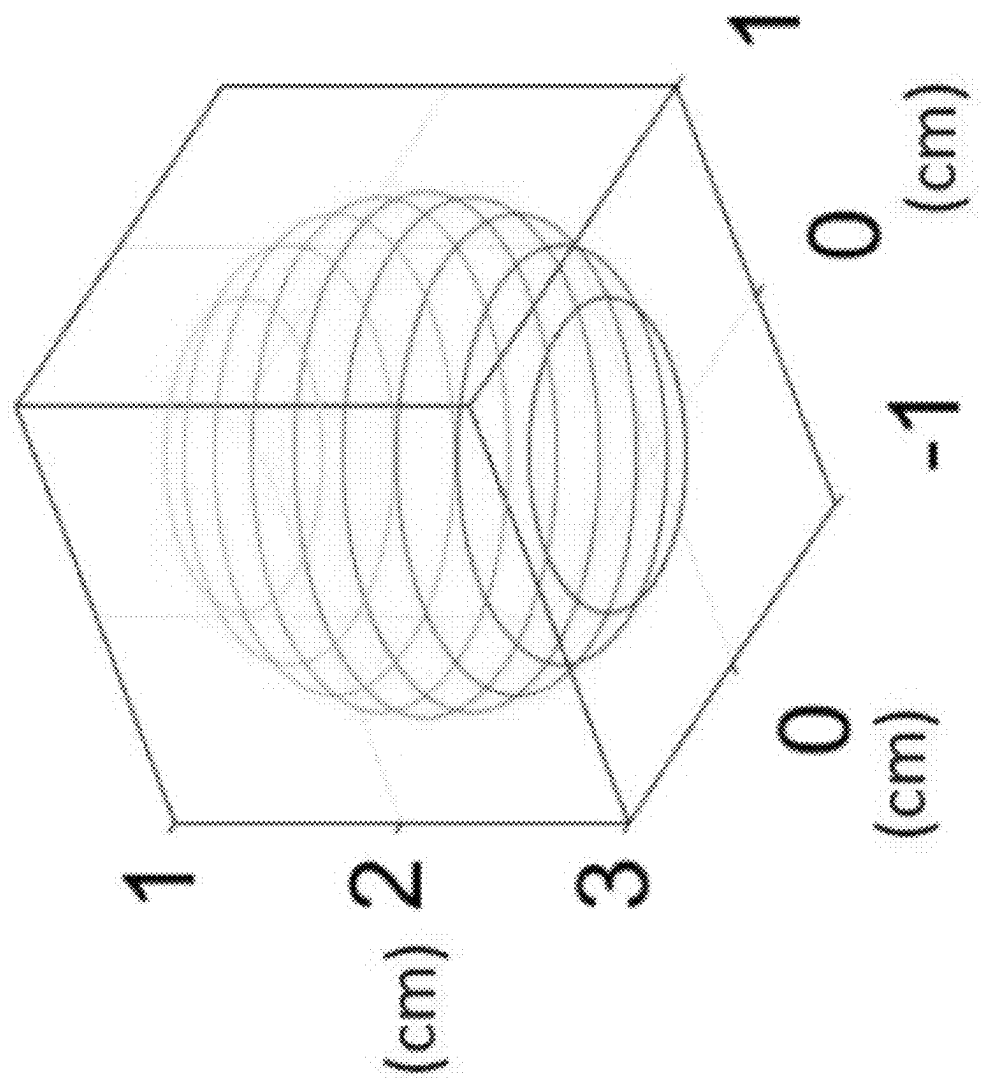


FIG. 4A

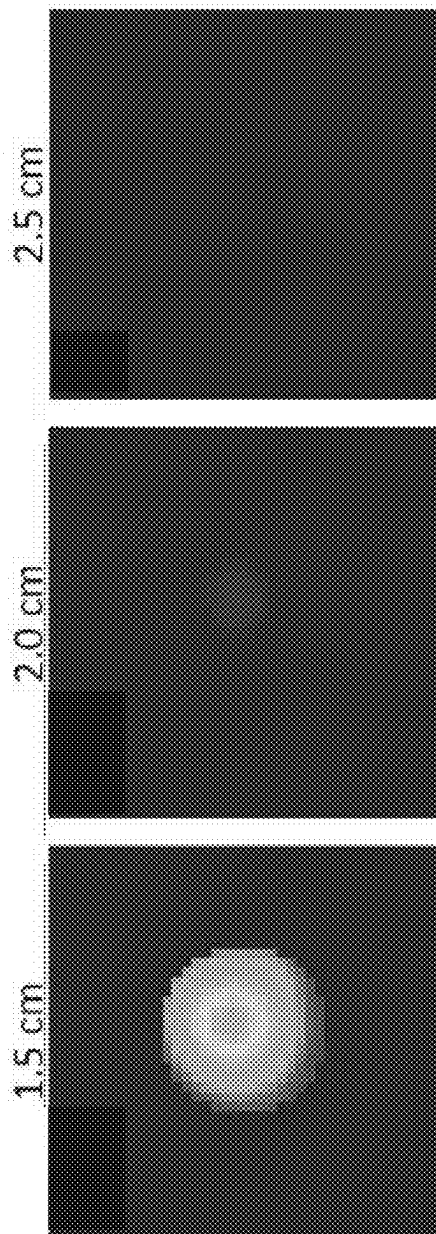


FIG. 4B

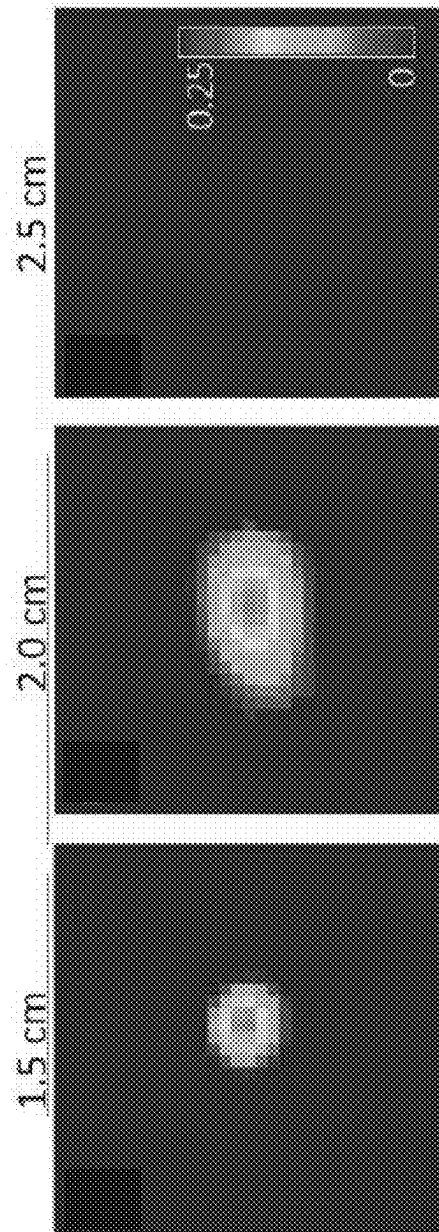


FIG. 4C

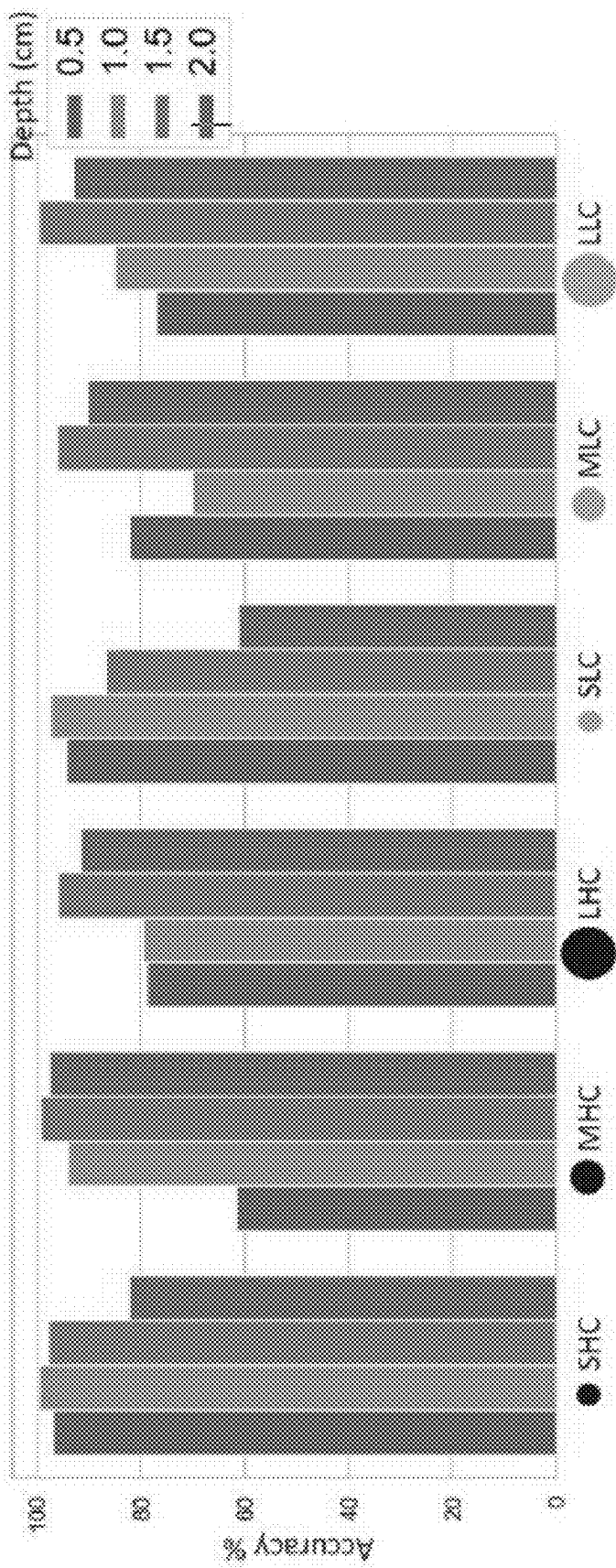


FIG. 5

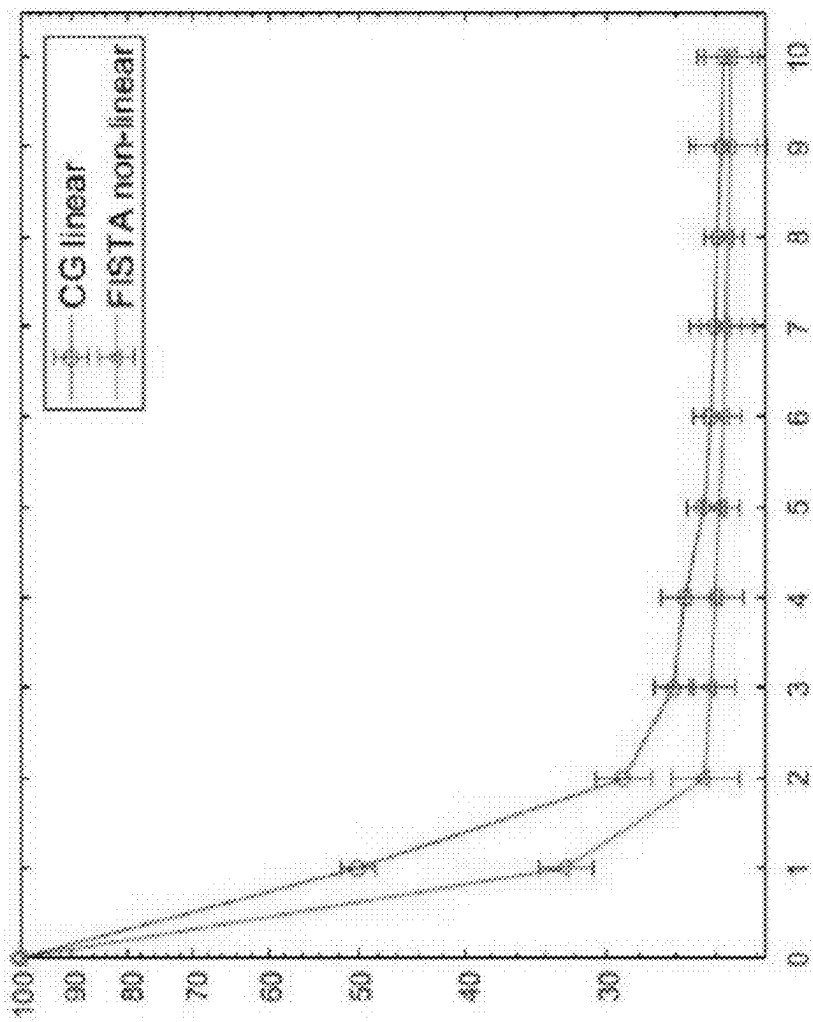


FIG. 6B

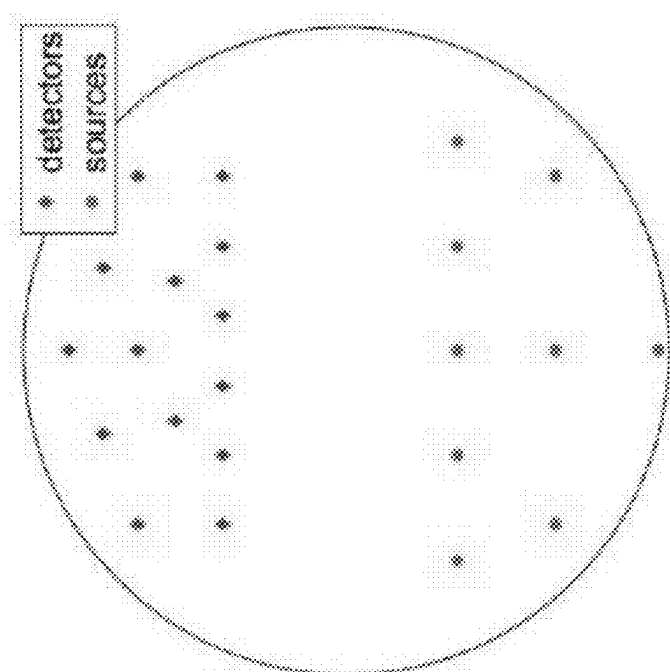


FIG. 6A

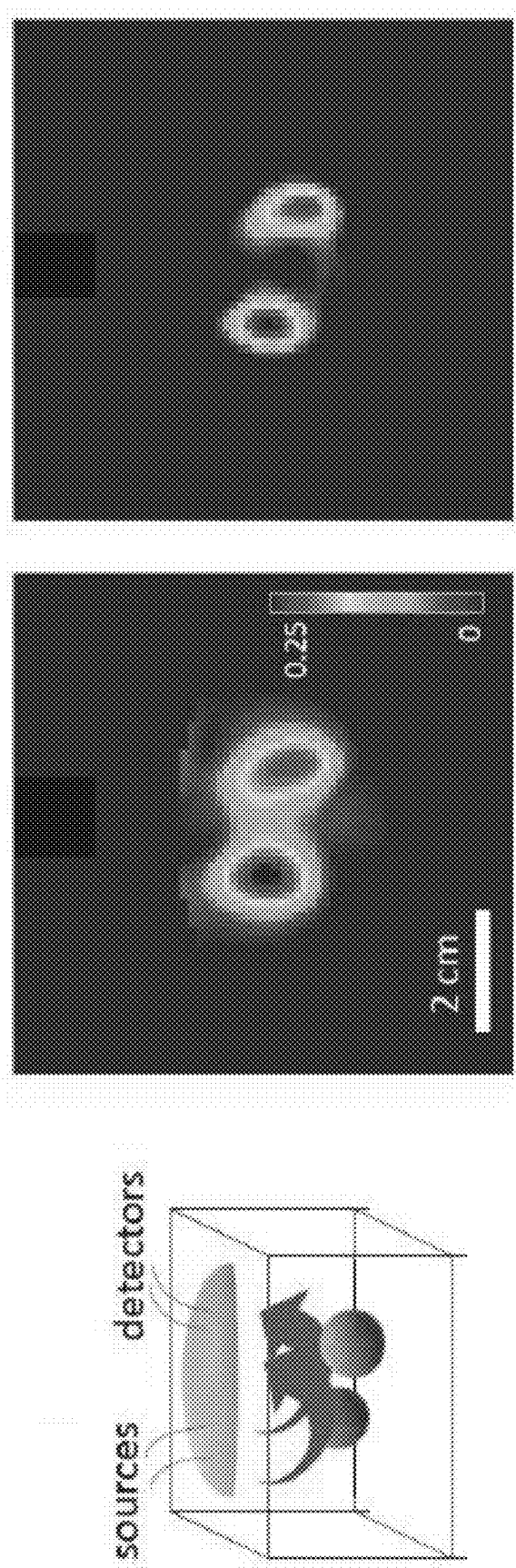


FIG. 7

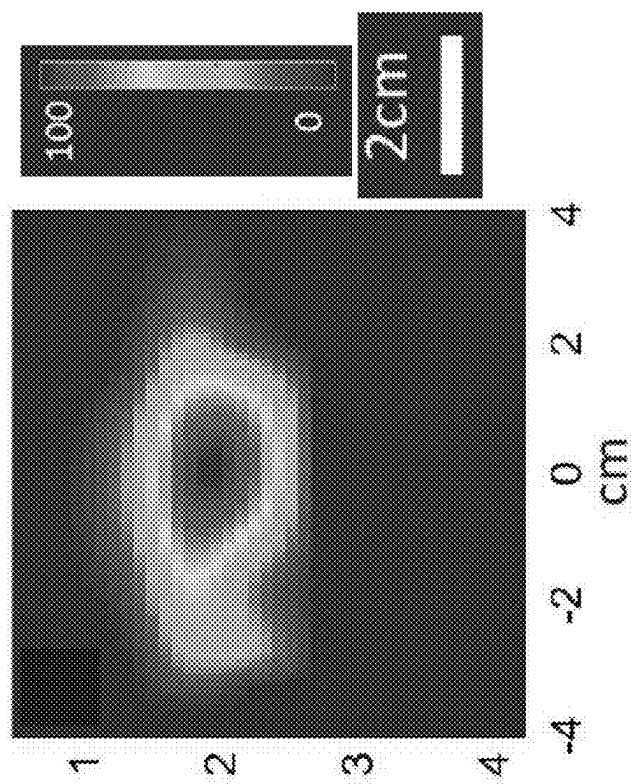


FIG. 8B

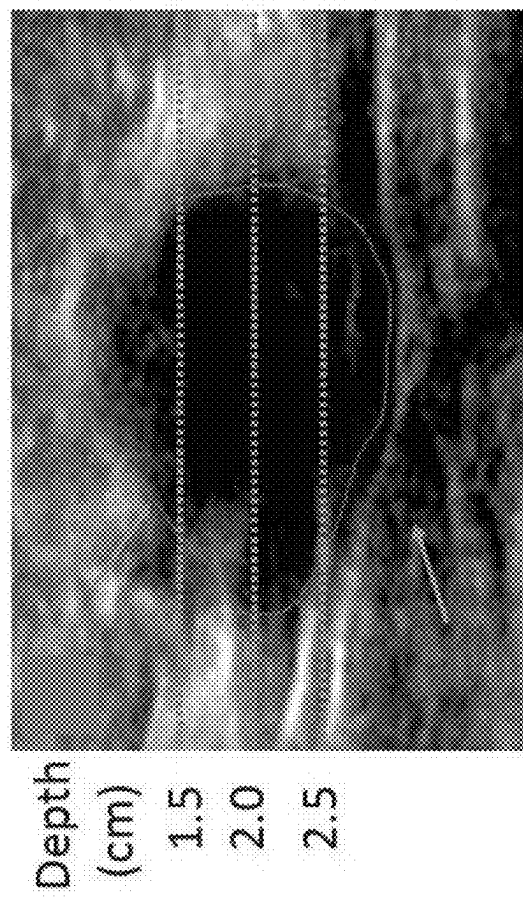
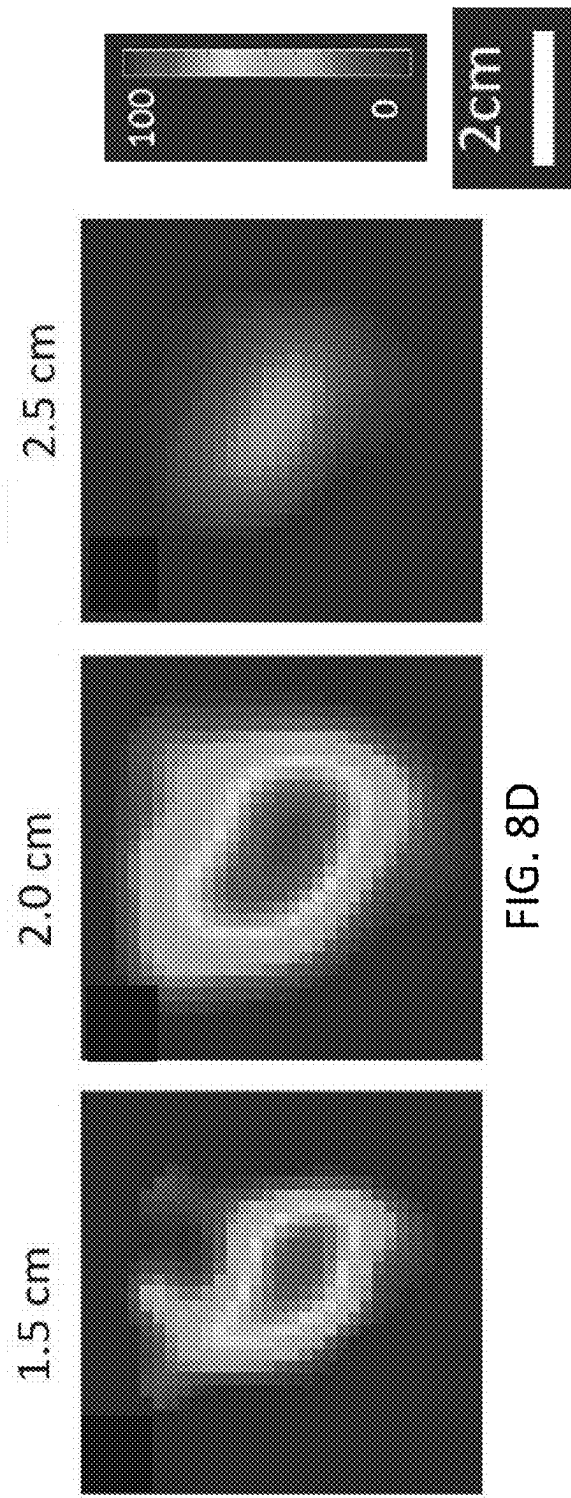
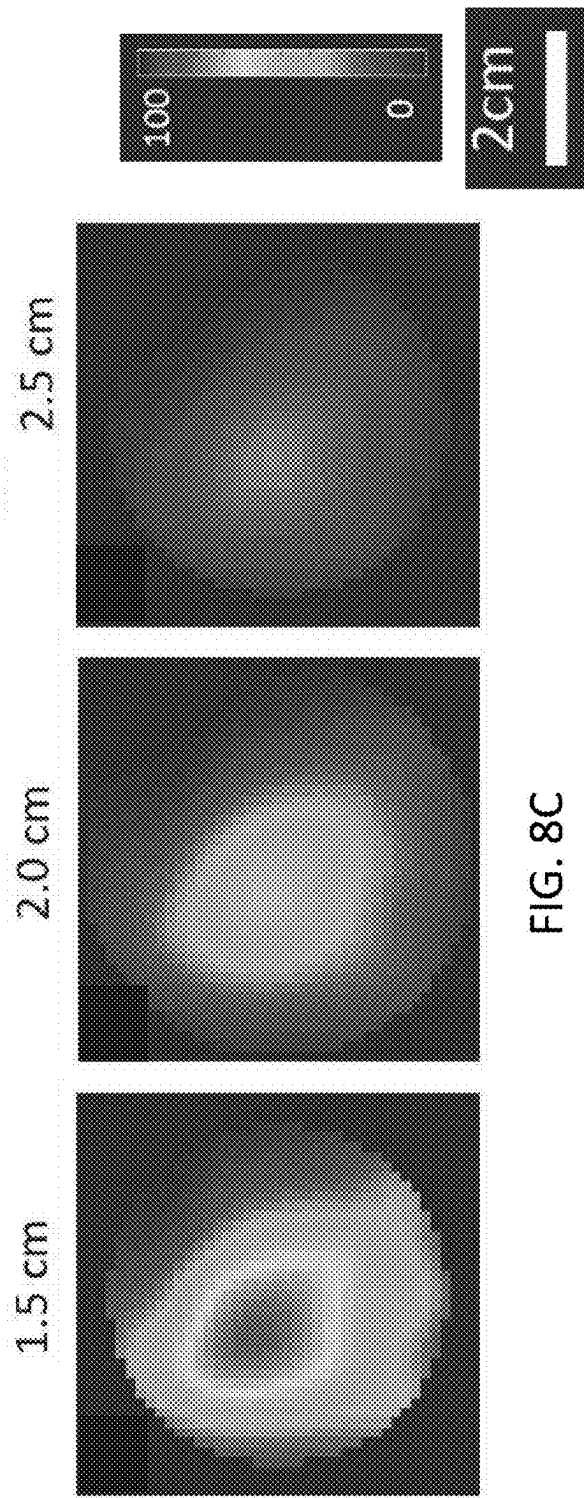


FIG. 8A



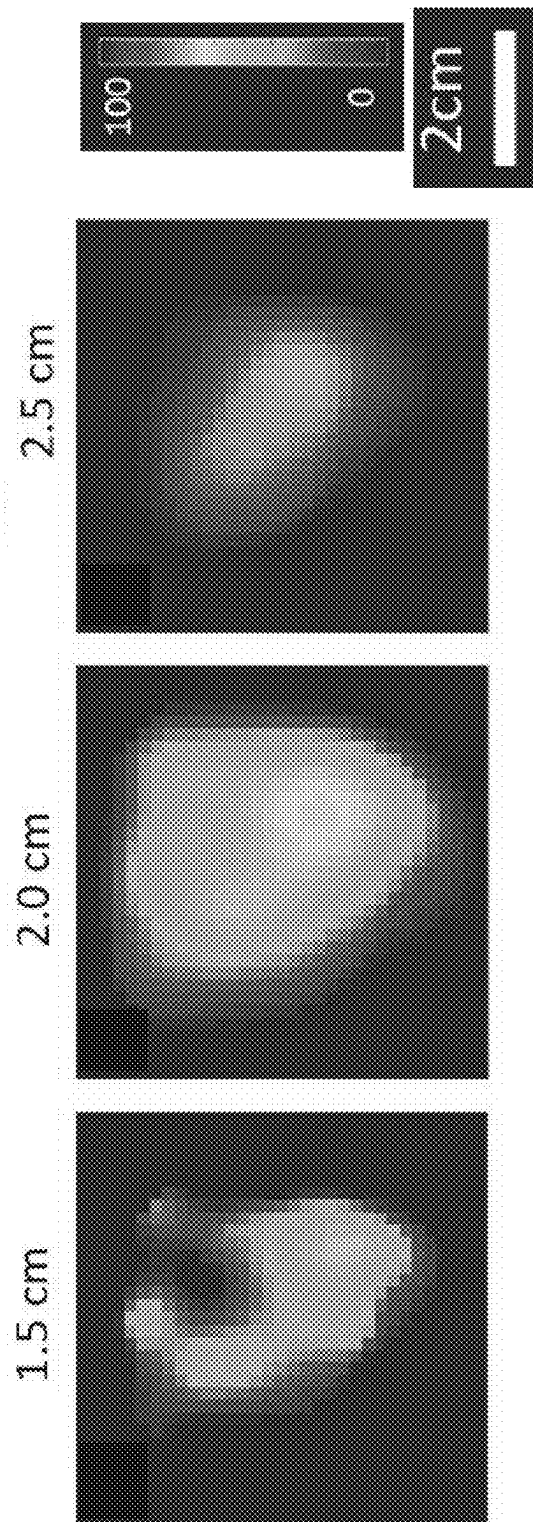


FIG. 8E

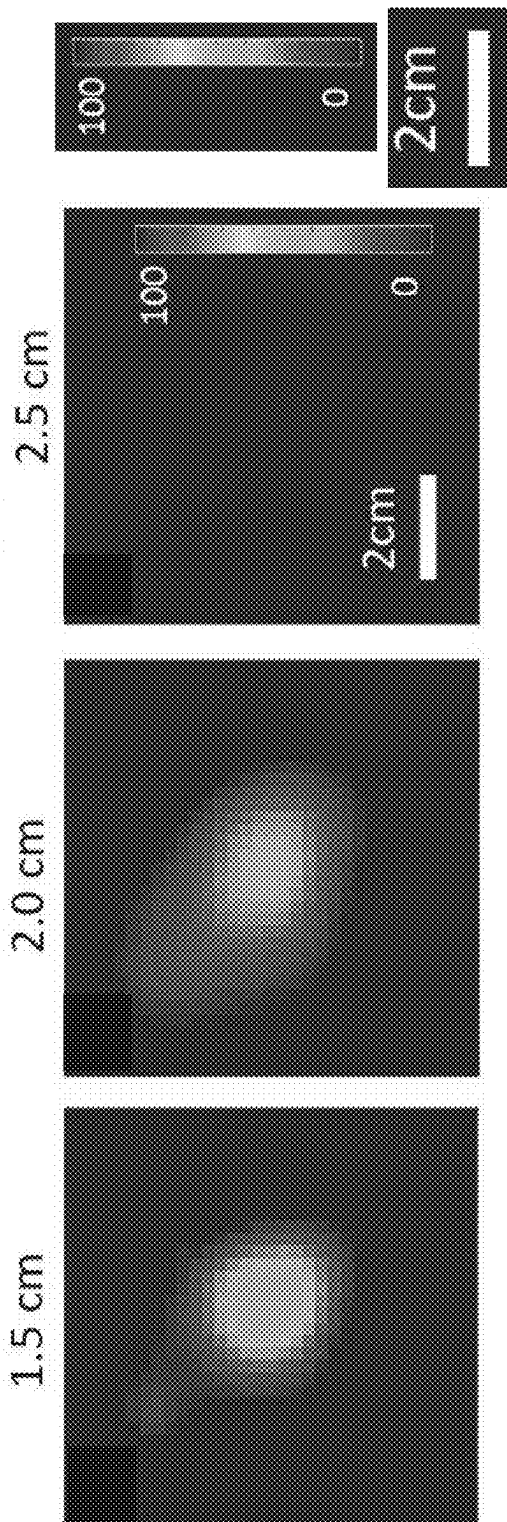


FIG. 8F

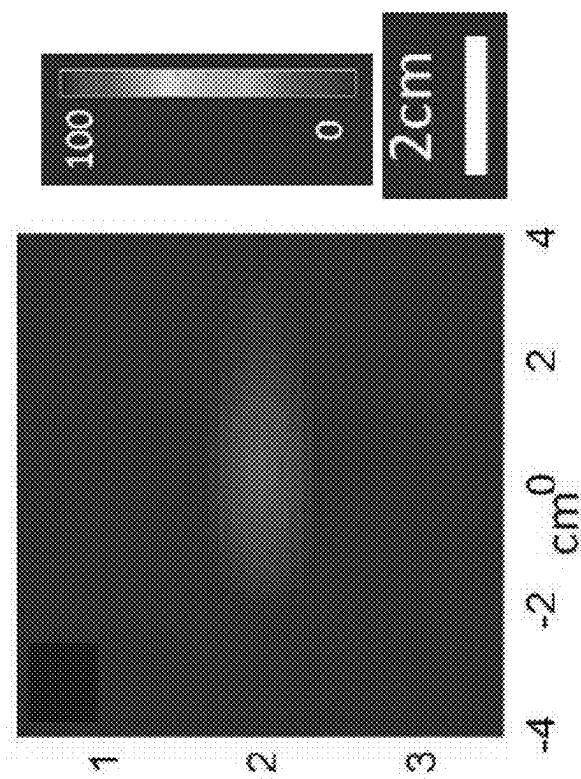


FIG. 9B

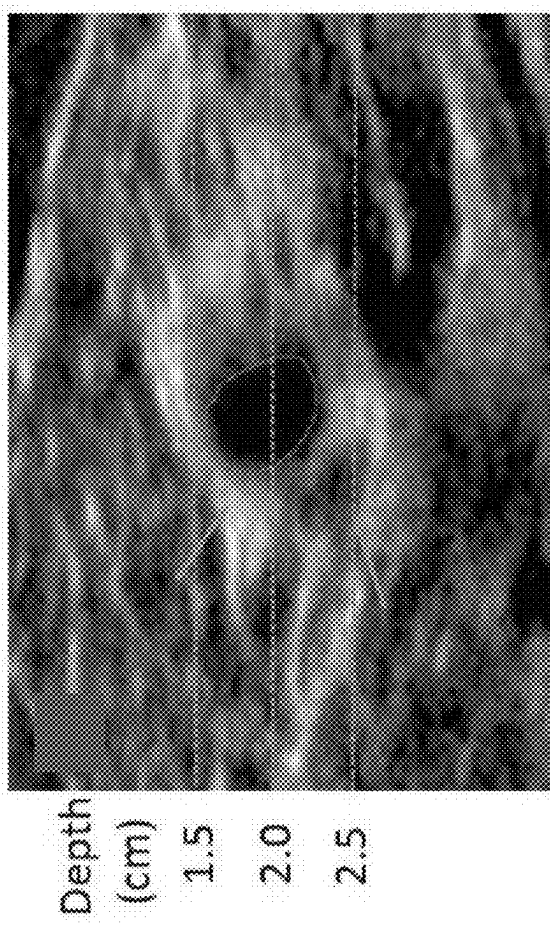


FIG. 9A

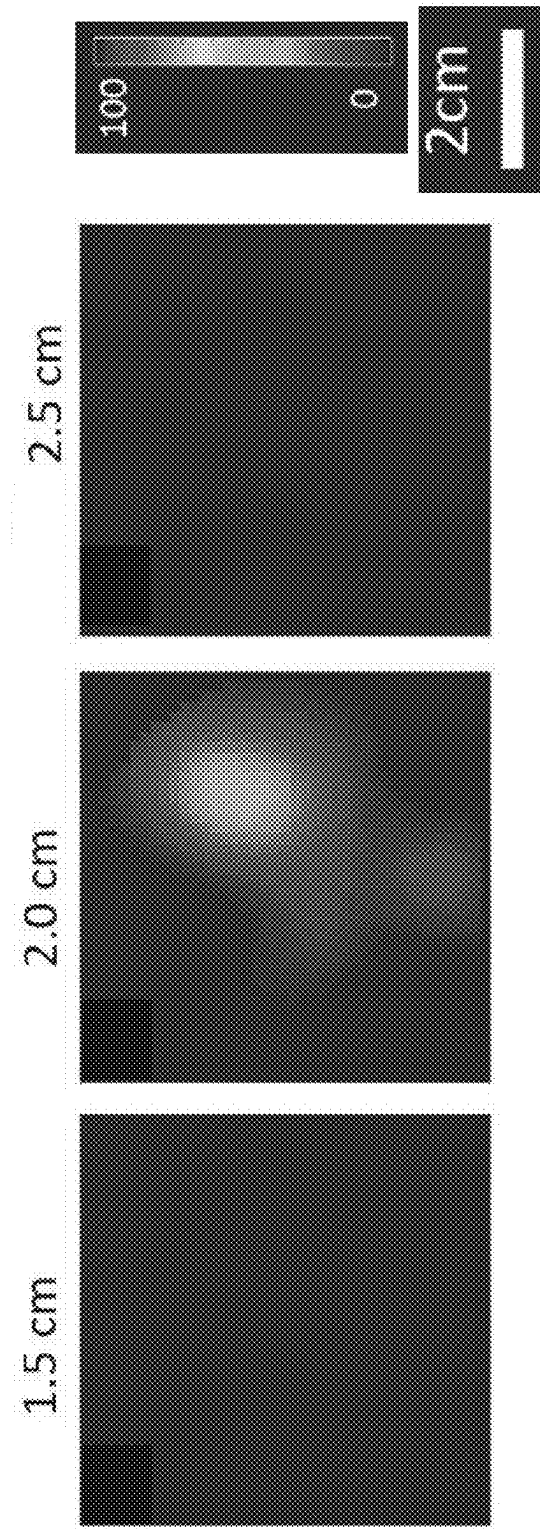


FIG. 9C

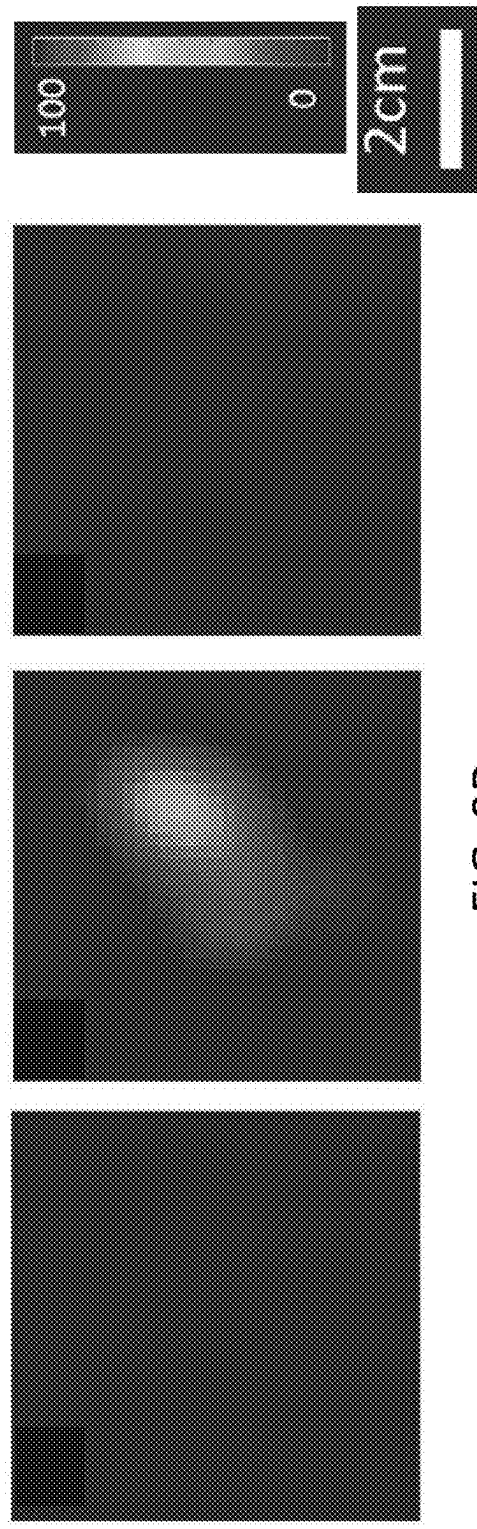
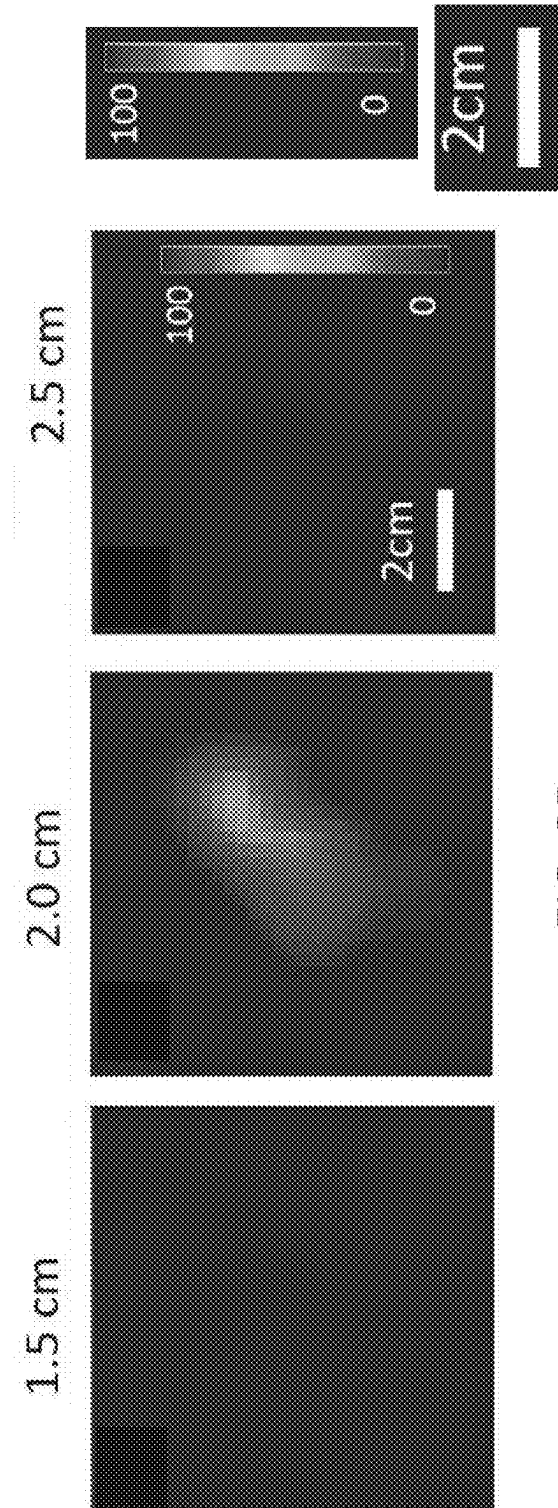
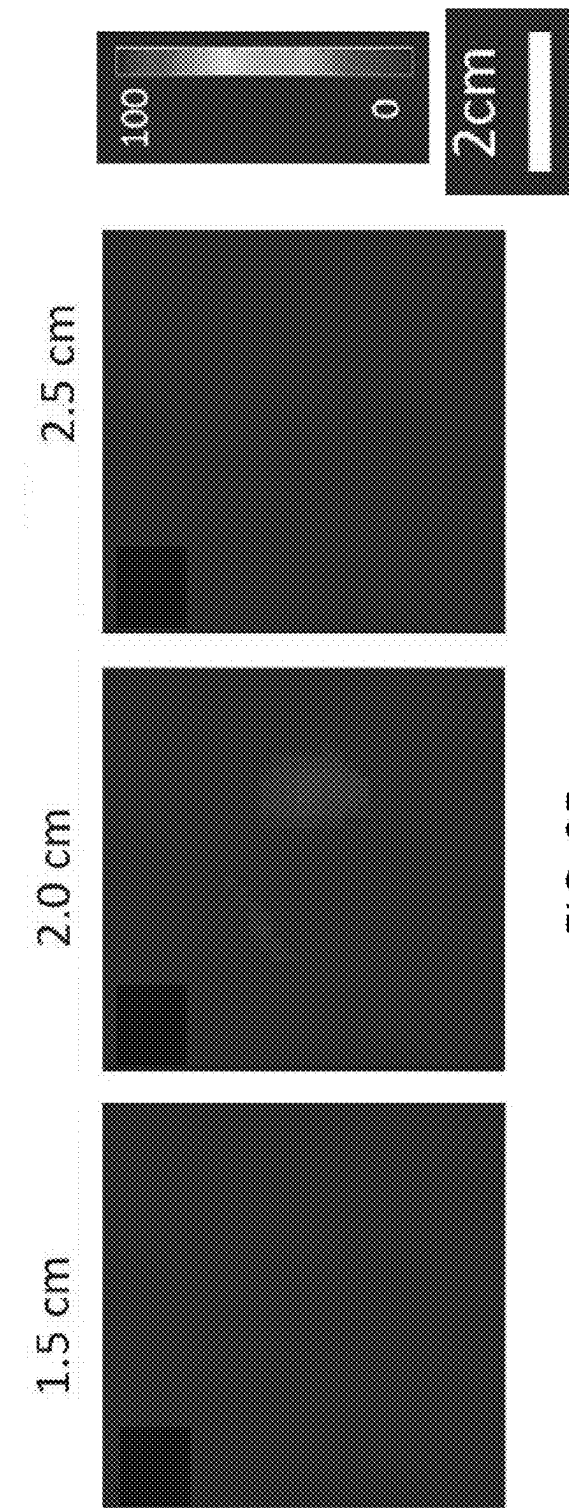


FIG. 9D



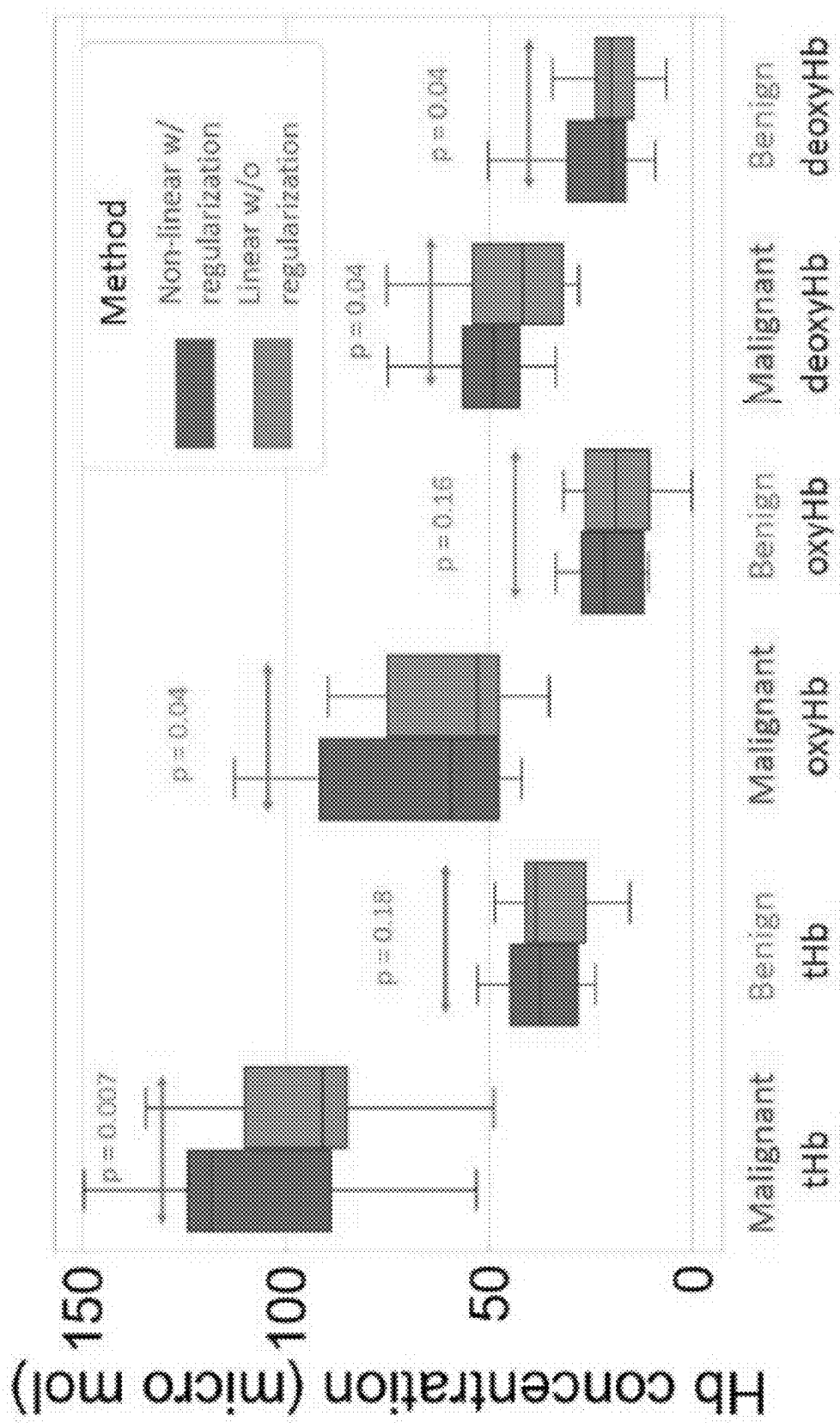


FIG. 10

depths of 0.5, 1.0, 1.5, and 2.0 cm were submerged. These depths were measured at the surface of the target using co-registered US images. The intralipid solution had an absorption coefficient $\mu_{\text{a0}}=0.02-0.03 \text{ cm}^{-1}$ and a reduced scattering coefficient $\mu_s=7-8 \text{ cm}^{-1}$, which were acquired by fitting.

The resolution of the proposed algorithm was explored by submerging two 1.0 cm diameter high contrast ($\mu_a=0.23 \text{ cm}^{-1}$) spherical targets inside the intralipid solution at 1.5 cm depth. The two balls were both placed in the center region along the US B-scan direction. Finally, the performance of the proposed algorithm was tested using data from 20 patients, of which 10 patients had malignant lesions, and 10 patients had benign lesions, based on biopsy results. Both the lesion and the normal contralateral breast were imaged with the US-guided DOT system. Measurements from the contralateral normal breast were used to estimate the average background optical properties of the breast.

Phantom experiments were performed with the methods described above. Reconstruction results were compared with the known first order linear Born method. FIG. 4A shows a 3D contour plot of the phantom target and FIG. 4B-4C show reconstructed images of a high optical contrast ball phantom located at 1.5 cm (top surface) depth inside the intralipid solution. The 3D absorption distribution is displayed as slices at different depths, labeled above each column: FIG. 4B is reconstruction of one 2 cm diameter ball using linear Born ($\mu_{\text{a max}}=0.18 \text{ cm}^{-1}$) and FIG. 4C is reconstruction of one 2 cm diameter ball using a non-linear Born ($\mu_{\text{a max}}=0.22 \text{ cm}^{-1}$). A more comprehensive analysis of the accuracy of absorption coefficients is shown in FIG. 5. HC and LC stand for high contrast ($\mu_a=0.23 \text{ cm}^{-1}$) and low contrast ($\mu_a=0.11 \text{ cm}^{-1}$), respectively. S, M, and L stand for small (1 cm diameter), medium (2 cm), and large (3 cm), respectively. The bars in the right upper legend indicate the depth of the top layer of the phantom target. The average absorption coefficients were estimated with 89.6% accuracy for high contrast phantoms and 86.1% for low contrast phantoms. The accuracy is calculated as $\mu_{\text{a max}}/\mu_{\text{a truth}} \times 100\%$.

FIG. 6A shows the schematic of the probe used for phantom experiments. The iterative image reconstruction method using phantom data shown in FIG. 5 is analyzed for convergence. To compare the method with the conjugate gradient optimization method for linear Born, the least squares error (LSE) was normalized for each method to the power of the scattered field, $\|y\|^2$. The mean and standard deviation of least square errors (LSE) for each method are plotted as a function of iterations shown in FIG. 6B, where zero initialization is used for both methods. FISTA converges faster than the conjugate gradient method. On average, the objective function converges to a lower value for non-linear modeling, because more accurate estimation of the photon-density wave better fits the perturbed photon-density wave measurement $U_{\text{sc}}(\mathbf{r})$ in Eq. (3), reducing the LSE.

Additionally, the resolution of reconstruction from non-linear Born with that from linear Born were compared by submerging two 1.0 cm diameter high contrast ($\mu_a=0.23 \text{ cm}^{-1}$) ball shaped targets separated by 2 cm along the US B-scan direction inside the intralipid solution at 1.5 cm depth. FIG. 7 illustrates the experiment (left) and the reconstruction results using linear Born without regularization (middle) and non-linear Born with regularization (right). The non-linear Born algorithm with sparse regularization gives a smaller full width at half maximum (FWHM) value,

which resolves the two targets much better than linear Born. This method does not require employing of two fine-grid regions, as discussed above.

Non-linear Born was compared with linear Born across 20 patients, 10 with benign lesions and 10 with malignant ones. Patient data were acquired from the lesion side of the breast and the contralateral mirror position of the healthy breast. The perturbed photo-density wave was calculated as

$$\frac{U_{\text{lesion}} - U_{\text{reference}}}{U_{\text{reference}}}, \quad \text{Eq. (14)}$$

where U_{lesion} and $U_{\text{reference}}$ are measurements from the lesion and reference breast, respectively. In the past, the use of a contralateral mirror position of a lesion breast were compared to a symmetric area of the same lesion breast as a healthy breast reference; however, the contralateral refer-

ence is more robust because the tissue curvature and the chest wall depth can be made symmetrical under the real-time assessment of co-registered ultrasound. FIG. 8A-8F show a reconstructed tHb, oxyHb, and deoxyHb map of a medium size malignant lesion. The tHb is calculated from absorption coefficients of four wavelengths, with the extinction coefficients for deoxygenated and oxygenated hemoglobin given in the literature. A co-registered US image is shown in FIG. 8A and indicates that the lesion is centered at 2 cm depth from the surface of the breast. A center slice of

the reconstructed tHb distribution at the orthogonal plane is shown in FIG. 8B. The functional maximum tHb concentration reconstructed with non-linear Born and linear Born are $95.0 \mu\text{M}$ and $84.4 \mu\text{M}$, respectively. FIG. 8C shows reconstructed tHb concentration distributions using linear Born without regularization at maximum tHb= $84.4 \mu\text{M}$. FIG. 8D shows reconstructed tHb concentration distributions using non-linear Born with regularization at maximum tHb= $95.0 \mu\text{M}$. FIG. 8E shows reconstructed oxyHb concentration distributions using non-linear Born with regularization at maximum oxyHb= $65.33 \mu\text{M}$. FIG. 8F shows recon-

structed deoxyHb concentration distributions using non-linear Born with regularization at maximum deoxyHb= $47.88 \mu\text{M}$. The oxyHb distribution closely follows the tHb distribution, but is more heterogeneous, with slightly periphery enhancement. The deoxyHb distribution is more centered in the tumor core. This type of peripheral oxyHb distribution and core deoxyHb distribution is often seen in larger cancers due to the necrotic tissue in the center and rapid tumor growth at the periphery. FIG. 9A-9F show reconstruction results on a benign lesion, and the co-registered US image, as shown in FIG. 9A, suggests the lesion is located at 2 cm depth. The maximum tHb concentrations reconstructed with non-linear Born and linear Born are $29.8 \mu\text{M}$ and $28.7 \mu\text{M}$, respectively. A center slice of the recon-

structed tHb distribution at the orthogonal plane is shown in FIG. 9B. FIG. 9C shows reconstructed tHb concentration distributions using linear Born without regularization at maximum tHb= $28.7 \mu\text{M}$. FIG. 9D shows reconstructed tHb concentration distributions using non-linear Born with regularization at maximum tHb= $29.8 \mu\text{M}$. FIG. 9E shows reconstructed oxyHb concentration distributions using non-linear Born with regularization at maximum oxyHb= $8.2 \mu\text{M}$. FIG. 9F shows reconstructed deoxyHb concentration distributions using non-linear Born with regularization at maximum deoxyHb= $25.3 \mu\text{M}$. It is interesting to note that this benign lesion had higher deoxyHb than oxyHb, but both are low. This benign lesion is diagnosed as a proliferate lesion, which

may account for the relatively higher deoxyHb component. Finally, the tHb, oxyHb, and deoxyHb values across all 20 cases were calculated. FIG. 10 illustrates the statistics of the reconstructed functional maximum tHb, oxyHb, and deoxyHb values in box plots. Again, non-linear Born is compared with linear Born. The non-linear Born algorithm improves the average malignant-to-benign lesion contrast ratio from 2.73 to 3.07, which is a 12.5% improvement. 12.4% improvement. For oxyHb and deoxyHb, the non-linear Born algorithm does not improve the average malignant-to-benign lesion ratio than that of linear Born. However, the mean oxyHb of non-linear Born of malignant group is higher than that of the linear Born ($p=0.04$), where p is the p-value from the t-test. The mean oxyHb of non-linear Born of benign group is statistically the same as the linear Born ($p=0.16$). This suggests that non-linear Born statistically improves the linear Born on oxyHb estimate for malignant group. For deoxyHb, non-linear Born improves deoxyHb than linear Born for both malignant and benign groups.

It has been experimentally demonstrated and validated that the proposed method can successfully reconstruct functional images of phantom targets and breast lesions. Phantom experiments confirm that the non-linear Born method yields better resolution and more accurate absorption coefficient distributions than the linear Born method.

In clinical cases, it is seen that non-linear Born reconstructs higher absorption coefficient value for large malignant cases than the linear Born method. Based on the results from 20 patients' data, the average malignant-to-benign lesion contrast is increased from 2.73, using the linear Born method, to 3.07, which is a 12.5% improvement. For lesions approximately more than 2.0 cm in diameter, the average malignant-to-benign contrast is increased from 2.68 to 3.31, which is a 23.5% improvement. This method can achieve more faithful results than the linear Born method because the photon-density wave attenuation is calculated more accurately with the iterative update, and the US a priori structure information is incorporated adequately through sparsity-promoting regularization. Moreover, the method also presents more realistic tumor absorption distributions.

To conclude, the proposed non-linear Born method with US-guided shape regularization significantly improves the reconstructed target shape, accuracy, and resolution. The method uses a non-linear forward model for better photon-density distribution estimation and a fast converging algorithm for solving the inverse problem, incorporating lesion structure information provided by the US image. Moreover, with selective modifications, the method is also applicable to MRI- or X-ray-guided DOT.

Embodiments of the disclosure, such as non-linear Born method with US-guided depth regularization may be described in the general context of computer-executable instructions, such as program modules, executed by one or more computers or other devices. The computer-executable instructions may be organized into one or more computer-executable components or modules. Generally, program modules include, but are not limited to, routines, programs, objects, components, and data structures that perform particular tasks or implement particular abstract data types. Aspects of the disclosure may be implemented with any number and organization of such components or modules. For example, aspects of the disclosure are not limited to the specific computer-executable instructions or the specific components or modules illustrated in the figures and described herein. Other embodiments of the disclosure may include different computer-executable instructions or components having more or less functionality than illustrated

and described herein. Aspects of the disclosure may also be practiced in distributed computing environments where tasks are performed by remote processing devices that are linked through a communications network. In a distributed computing environment, program modules may be located in both local and remote computer storage media including memory storage devices.

The computer systems, computing devices, and computer-implemented methods discussed herein may include 10 additional, less, or alternate actions and/or functionalities, including those discussed elsewhere herein. The computer systems may include or be implemented via computer-executable instructions stored on non-transitory computer-readable media. The methods may be implemented via one 15 or more local or remote processors, transceivers, servers, and/or sensors (such as processors, transceivers, servers, and/or sensors mounted on vehicle or mobile devices, or associated with smart infrastructure or remote servers), and/or via computer executable instructions stored on non-transitory computer-readable media or medium.

In some aspects, a computing device is configured to implement machine learning, such that the computing device "learns" to analyze, organize, and/or process data without being explicitly programmed. Machine learning 20 may be implemented through machine learning (ML) methods and algorithms. In one aspect, a machine learning (ML) module is configured to implement ML methods and algorithms. In some aspects, ML methods and algorithms are applied to data inputs and generate machine learning (ML) 25 outputs. Data inputs may include but are not limited to: images or frames of a video, object characteristics, and object categorizations. Data inputs may further include: sensor data, image data, video data, telematics data, authentication data, authorization data, security data, mobile device 30 data, geolocation information, transaction data, personal identification data, financial data, usage data, weather pattern data, "big data" sets, and/or user preference data. ML outputs may include but are not limited to: a tracked shape output, categorization of an object, categorization of a type 35 of motion, a diagnosis based on motion of an object, motion analysis of an object, and trained model parameters. ML outputs may further include: speech recognition, image or 40 video recognition, medical diagnoses, statistical or financial models, autonomous vehicle decision-making models, robotics behavior modeling, fraud detection analysis, user 45 recommendations and personalization, game AI, skill acquisition, targeted marketing, big data visualization, weather forecasting, and/or information extracted about a computer device, a user, a home, a vehicle, or a party of a transaction. In some aspects, data inputs may include certain ML 50 outputs.

In some aspects, at least one of a plurality of ML methods and algorithms may be applied, which may include but are not limited to: linear or logistic regression, instance-based 55 algorithms, regularization algorithms, decision trees, Bayesian networks, cluster analysis, association rule learning, artificial neural networks, deep learning, dimensionality reduction, and support vector machines. In various aspects, the implemented ML methods and algorithms are directed toward at least one of a plurality of categorizations of machine learning, such as supervised learning, unsupervised learning, and reinforcement learning.

In one aspect, ML methods and algorithms are directed 60 toward supervised learning, which involves identifying patterns in existing data to make predictions about subsequently received data. Specifically, ML methods and algorithms directed toward supervised learning are "trained" through 65

training data, which includes example inputs and associated example outputs. Based on the training data, the ML methods and algorithms may generate a predictive function which maps outputs to inputs and utilize the predictive function to generate ML outputs based on data inputs. The example inputs and example outputs of the training data may include any of the data inputs or ML outputs described above. For example, a ML module may receive training data comprising customer identification and geographic information and an associated customer category, generate a model which maps customer categories to customer identification and geographic information, and generate a ML output comprising a customer category for subsequently received data inputs including customer identification and geographic information.

In another aspect, ML methods and algorithms are directed toward unsupervised learning, which involves finding meaningful relationships in unorganized data. Unlike supervised learning, unsupervised learning does not involve user-initiated training based on example inputs with associated outputs. Rather, in unsupervised learning, unlabeled data, which may be any combination of data inputs and/or ML outputs as described above, is organized according to an algorithm-determined relationship. In one aspect, a ML module receives unlabeled data comprising customer purchase information, customer mobile device information, and customer geolocation information, and the ML module employs an unsupervised learning method such as "clustering" to identify patterns and organize the unlabeled data into meaningful groups. The newly organized data may be used, for example, to extract further information about a customer's spending habits.

In yet another aspect, ML methods and algorithms are directed toward reinforcement learning, which involves optimizing outputs based on feedback from a reward signal. Specifically ML methods and algorithms directed toward reinforcement learning may receive a user-defined reward signal definition, receive a data input, utilize a decision-making model to generate a ML output based on the data input, receive a reward signal based on the reward signal definition and the ML output, and alter the decision-making model so as to receive a stronger reward signal for subsequently generated ML outputs. The reward signal definition may be based on any of the data inputs or ML outputs described above. In one aspect, a ML module implements reinforcement learning in a user recommendation application. The ML module may utilize a decision-making model to generate a ranked list of options based on user information received from the user and may further receive selection data based on a user selection of one of the ranked options. A reward signal may be generated based on comparing the selection data to the ranking of the selected option. The ML module may update the decision-making model such that subsequently generated rankings more accurately predict a user selection.

As will be appreciated based upon the foregoing specification, the above-described aspects of the disclosure may be implemented using computer programming or engineering techniques including computer software, firmware, hardware or any combination or subset thereof. Any such resulting program, having computer-readable code means, may be embodied or provided within one or more computer-readable media, thereby making a computer program product, i.e., an article of manufacture, according to the discussed aspects of the disclosure. The computer-readable media may be, for example, but is not limited to, a fixed (hard) drive, diskette, optical disk, magnetic tape, semiconductor memory

such as read-only memory (ROM), and/or any transmitting/receiving medium, such as the Internet or other communication network or link. The article of manufacture containing the computer code may be made and/or used by executing the code directly from one medium, by copying the code from one medium to another medium, or by transmitting the code over a network.

Definitions and methods described herein are provided to better define the present disclosure and to guide those of ordinary skill in the art in the practice of the present disclosure. Unless otherwise noted, terms are to be understood according to conventional usage by those of ordinary skill in the relevant art.

In some embodiments, numbers expressing quantities of ingredients, properties such as molecular weight, reaction conditions, and so forth, used to describe and claim certain embodiments of the present disclosure are to be understood as being modified in some instances by the term "about." In some embodiments, the term "about" is used to indicate that a value includes the standard deviation of the mean for the device or method being employed to determine the value. In some embodiments, the numerical parameters set forth in the written description and attached claims are approximations that can vary depending upon the desired properties sought to be obtained by a particular embodiment. In some embodiments, the numerical parameters should be construed in light of the number of reported significant digits and by applying ordinary rounding techniques. Notwithstanding that the numerical ranges and parameters setting forth the broad scope of some embodiments of the present disclosure are approximations, the numerical values set forth in the specific examples are reported as precisely as practicable. The numerical values presented in some embodiments of the present disclosure may contain certain errors necessarily resulting from the standard deviation found in their respective testing measurements. The recitation of ranges of values herein is merely intended to serve as a shorthand method of referring individually to each separate value falling within the range. Unless otherwise indicated herein, each individual value is incorporated into the specification as if it were individually recited herein.

In some embodiments, the terms "a" and "an" and "the" and similar references used in the context of describing a particular embodiment (especially in the context of certain of the following claims) can be construed to cover both the singular and the plural, unless specifically noted otherwise. In some embodiments, the term "or" as used herein, including the claims, is used to mean "and/or" unless explicitly indicated to refer to alternatives only or the alternatives are mutually exclusive.

The terms "comprise," "have" and "include" are open-ended linking verbs. Any forms or tenses of one or more of these verbs, such as "comprises," "comprising," "has," "having," "includes" and "including," are also open-ended. For example, any method that "comprises," "has" or "includes" one or more steps is not limited to possessing only those one or more steps and can also cover other unlisted steps. Similarly, any composition or device that "comprises," "has" or "includes" one or more features is not limited to possessing only those one or more features and can cover other unlisted features.

All methods described herein can be performed in any suitable order unless otherwise indicated herein or otherwise clearly contradicted by context. The use of any and all examples, or exemplary language (e.g. "such as") provided with respect to certain embodiments herein is intended merely to better illuminate the present disclosure and does

21

tion method regularized by the depth dependent ℓ_1 regularization associated with the initial estimate, by:

- (1) generating, as part of the functional image, a lesion absorption map based on the initial estimate by solving the inverse optimization problem with the target-shape-regularized FISTA;
- (2) updating, using a Finite Difference Method (FDM), a photon-density wave distribution associated with the initial estimate to obtain an updated estimation of a weight matrix for use with the depth dependent ℓ_1 regularized non-linear Born iterative reconstruction method;
- (3) generating an updated weight matrix based at least on the updated estimation of the weight matrix; and
- (4) performing at least two iterations of the depth dependent ℓ_1 regularized non-linear Born iterative reconstruction method, at least one of the at least two iterations using the updated weight matrix; and

displaying the generated functional image.

8. The method of claim 7, further comprising calculating an initial estimate of the functional image using a dual-grid schedule to discretize the lesion region with a fine grid and to discretize the background volume of the subject with a coarse grid to generate a weighted matrix for the lesion region and a weighted matrix for the background volume based on absorption of the optical waves on the subject.

9. The method of claim 8, further comprising performing reconstructing via the depth dependent ℓ_1 regularized non-linear Born iterative reconstruction method for generating the functional image iteratively by updating the photon-density wave distribution with a conjugate gradient method inside the fine grid.

10. The method of claim 7, further comprising generating optical waves at four optical wavelengths in a range from 730 nm to 830 nm.

11. The method of claim 7, wherein the depth dependent ℓ_1 regularized non-linear Born iterative reconstruction method is configured to reconstruct at least one of values or distributions of absorption coefficients associated with absorption of the optical waves on the subject.

12. At least one non-transitory computer-readable storage media having computer-executable instructions embodied thereon for generating a functional image of a lesion region of a subject using diffuse optical tomography (DOT), wherein when executed by at least one processor, the computer-executable instructions cause the processor to:

- emit optical waves toward a lesion region of the subject;
- detect optical waves reflected by the lesion region and
- convert the optical waves to digital signals;
- receive lesion depth and shape information from a plurality of co-registered ultrasound images of the lesion region;
- calculate an initial estimate of the functional image based on the digital signals and the lesion depth and shape information by solving an inverse optimization problem with a shape-regularized Fast Iterative Shrinkage-Thresholding algorithm (FISTA), wherein the calculation of the initial estimate is based upon depth dependent ℓ_1 regularization;

22

generate the functional image of the lesion region of the subject by performing a depth dependent ℓ_1 regularized non-linear Born iterative reconstruction method that comprises non-linear Born iterative reconstruction method regularized by the depth dependent ℓ_1 regularization associated with the initial estimate, the functional image being generated by the processor being further caused by the computer-executable instructions to:

- (1) generate, as part of the functional image, a lesion absorption map based on the initial estimate by solving the inverse optimization problem with the target-shape-regularized FISTA;
 - (2) update, using a Finite Difference Method (FDM), a photon-density wave distribution associated with the initial estimate to obtain an updated estimation of a weight matrix for use with the depth dependent ℓ_1 regularized non-linear Born iterative reconstruction method;
 - (3) generate an updated weight matrix based at least on the updated estimation of the weight matrix; and
 - (4) perform at least two iterations of the depth dependent ℓ_1 regularized non-linear Born iterative reconstruction method, at least one of the at least two iterations using the updated weight matrix; and
- display the generated functional image.

13. The computer-readable storage medium of claim 12, wherein the computer-executable instructions further cause the processor to calculate an initial estimate of the functional image using a dual-grid schedule to discretize the lesion region with a fine grid and to discretize the background volume of the subject with a coarse grid to generate a weighted matrix for the lesion region and a weighted matrix for the background volume based on absorption of the optical waves on the subject.

14. The computer-readable storage medium of claim 13, wherein the computer-executable instructions further cause the processor to perform reconstruction via the depth dependent ℓ_1 regularized non-linear Born iterative reconstruction method for generating the functional image iteratively by updating the photon-density wave distribution with a conjugate gradient method inside the fine grid.

15. The computer-readable storage medium of claim 12, wherein the computer-executable instructions further cause the processor to receive the plurality of co-registered ultrasound images of the lesion region from an ultrasound imaging device.

16. The computer-readable storage medium of claim 12, wherein the computer-executable instructions further cause the processor to generate near-infrared (NIR) optical waves at four optical wavelengths in a range from 730 nm to 830 nm.

17. The computer-readable storage medium of claim 12, wherein the depth dependent ℓ_1 regularized non-linear Born iterative reconstruction method is configured to reconstruct at least one of values or distributions of absorption coefficients associated with absorption of the optical waves on the subject.

* * * * *